Available online at www.sciencedirect.com
ScienceDirect
International Journal of Heat and Mass Transfer 50 (2007) 3545–3555
International Journal of HEAT and MASS TRANSFER
www.elsevier.com/locate/ijhmt

An analytical model for heat and mass transfer processes in internally cooled or heated liquid desiccant–air contact units

Cheng Qin Ren *, Min Tu, Hua Hui Wang

College of Mechanical and Automotive Engineering, Hunan University, Changsha 410082, China

Received 22 February 2006; received in revised form 14 November 2006
Available online 27 March 2007

Abstract

Internally cooled or heated liquid desiccant–air contact units can be used for effective air dehumidification or desiccant regeneration, respectively. One-dimensional differential equations were utilized in the present study to describe the heat and mass transfer processes with parallel/counterflow configurations. The effects of solution film heat and mass transfer resistances, the variations of solution mass flow rate, non-unity values of Lewis factor and incomplete surface wetting conditions were all considered in the differential model. On considering the relatively narrow ranges of operating conditions in a specified application, the equilibrium humidity ratio of desiccant solution was assumed to be a linear function of its temperature and concentration. Constant approximations of some properties and coefficients were further made to render the coupled equations linear. The differential equations were rearranged and an analytical solution was developed for newly defined parameters. For four possible flow arrangements and three types of commonly used liquid desiccant solutions, results of analytical solutions were compared with those of numerical integrations over a wide range of operating conditions, and the agreement was found to be quite satisfactory. Further, the heat and mass transfer performances were analyzed and some guidance to improve the unit design was provided.

Keywords: Internally cooled or heated liquid desiccant–air contact units; Heat and mass transfer performances; One-dimensional model; Analytical solution

1. Introduction

Liquid desiccant cooling system driven by solar energy or other heat sources has been emerged as a potential alternative or as a supplement to conventional vapor compression (V-C) systems for cooling and air conditioning. Dehumidification and regeneration are the key processes. Internally cooled or heated liquid desiccant–air contact units have been widely concerned for their potential applications in effective air dehumidification, desiccant regeneration or high capacity energy storage systems [1–5].

The internally cooled or heated liquid desiccant–air contact units will generally be categorized either as coil-type [1–3,6–13] or plate type [14,15] heat and mass exchangers. In coil-type exchangers, the cooling or heating fluid flows inside the coil-tubes while the desiccant solution flows over the outer surface of the tube banks in direct contact with the air. The flow pattern of coil-type exchangers can be easily arranged as parallel/counterflow configurations [1–3,6–10]. Due to the difficulty in manufacturing, plate type exchangers are usually as crossflow pattern. Kessling et al. [4,5] designed and manufactured a new type of dehumidifiers where the cooling fluid flows inside the tube-like channels within double plates and the flow pattern is in generally parallel/countercurrent flow configurations. Jain et al. [16] tested a falling film tubular type of absorber, where both air and solution flow inside the tubes from top to bottom while the cooling water is circulated through the shell from bottom to top.

Different mathematical models have been developed for the internally cooled or heated liquid desiccant–air contact

* Corresponding author. Tel.: +86 138 74886953; fax: 86 731 8711911.
E-mail address: renchengqin@163.com (C.Q. Ren).

0017-9310/$ - see front matter © 2007 Elsevier Ltd. All rights reserved.
doi:10.1016/j.ijheatmasstransfer.2006.12.034

Nomenclature

a	interface area for heat transfer per unit length of the exchanger (m^2/m)
a_f	fluid-to-solution heat transfer area per unit length of the exchanger (m^2/m)
a_M	interface area for mass transfer per unit length of the exchanger (m^2/m)
$\mathbf{A}$	coefficients matrix in Eq. (25)
b_{ij}, k_{ij}	elements of coefficients matrices $\mathbf{B}$ and $\mathbf{K}$, respectively
B_0–B_2	constants in Eqs. (11) and (14) etc.
$\mathbf{B}$	coefficients matrix in Eq. (35)
c_p	specific heat capacity (kJ/ kg °C)
$c_{p,da}$	specific heat capacity of dry air (kJ/ kg °C)
C_s^*, C_f^*	solution and fluid to dry air heat capacity rate ratios, respectively
C_1–C_3	coefficients in Eq. (30)
d	a constant in Eq. (37)
D_0	a coefficient in Eq. (37)
e_t, e_ξ	coefficients in Eq. (15)
$\mathbf{e}(\mathrm{NTU_x})$	diagonal matrix defined in Eq. (34)
$\mathbf{E}$	identity matrix
$\mathbf{F}$	coefficients matrix in Eq. (39)
$\mathbf{g}$	constants vector in Eq. (39)
h	specific enthalpy (kJ/kg)
h_{ab}	heat of absorption or desorption $h_{ab} = h_v - \hat{h}_w$ (kJ/kg)
h_{DG}	interface-to-air convective mass transfer coefficient (kg/m^2 s)
h_{DL}	solution-to-interface convective mass transfer coefficient (kg/m^2 s)
$h_{fg,0}$	evaporation heat of pure water at reference temperature (0 °C) (kJ/kg)
$\bar{h}_{fg}$	a normalized heat of evaporation at reference condition (0 °C)
h_G	interface-to-air convective heat transfer coefficient (kW/m^2 °C)
h_L	solution-to-interface convective heat transfer coefficient (kW/m^2 °C)
$\hat{h}_w$	partial enthalpy of water in desiccant solution $\hat{h}_w = h_s - \xi\frac{\partial h_s}{\partial \xi}$ (kJ/kg)
$\mathbf{K}$	coefficients matrix in Eq. (30)
L_a, L_f, L_s	lengths in the directions of air, fluid and solution streams, respectively
Le_f	Lewis factor
$\dot{m}$	mass flow rate (kg/s)
m_R	air to solution mass flow rate ratio
NTU	number of air side heat transfer units
$\mathrm{NTU_x}$	dimensionless coordinate defined as $\mathrm{dNTU_x} = \mathrm{NTU}\mathrm{d}\bar{x}_s$
P_1–P_4	coefficients in Eqs. (18) and (19)
r	a ratio of heat transfer capacitances
R_{cv}	water vapor to dry air specific heat capacity ratio
R_h	air phase to solution phase heat transfer coefficients ratio
R_{hD}	air phase to solution phase mass transfer coefficients ratio
t	temperature (°C)
U	overall heat transfer coefficient between fluid and solution (kW/m^2 °C)
W	humidity ratio (kg/kg(a))
x_a, x_f, x_s	space coordinates originated from the inlets of air, fluid and solution streams, respectively
$\mathbf{Y}$	function variable vector defined in Eq. (26)

Greek symbols

Δ	change of or difference between parameters
δ_a, δ_f	flow direction indicators for air and fluid streams, respectively
ϑ	dimensionless temperatures defined in Eq. (23)
$\lambda_1 \sim \lambda_3$	roots of the characteristic equation
σ	surface wettability
ξ	desiccant concentration ($kg_{salt}/kg_{solution}$)

Subscripts

a	of air or on air side
av	averaged value
B	bottom position
e	of air in equilibrium with desiccant solution
f	of fluid stream
i	inlet
I	at interface
max	maximum value
min	minimum value
o	outlet
s	of, at or in equilibrium with bulk solution
T	top position
v	of water vapor
x	local position

Superscripts

a	of analytical results
n	results by numerical integration of the one dimensional differential equations

units. Generally, the bulk flow model of energy and mass balance equations for an air stream, a solution stream and a cooling or heating fluid stream were utilized to describe the heat and mass transfer performances. One-dimensional models were utilized for parallel/countercurrent flow configurations [1–10,16]. Two-dimensional models were developed by Khan et al. [12,13] for the cross flow type absorbers where the refrigerant or coolant water flows in counterflow direction to the process air and in cross-flow direction to the solution. More complicated

differential models [14,17] concerns with the absorption processes coupled with evaporative cooling in the alternative channels. Heat and mass transfer resistances between the bulk film of solution and the film surface were often neglected [4–10,12–14,16,17]. Thus overall gas phase heat and mass transfer coefficients should better be utilized to obtain more accurate simulation results. In Hellmann and Grossman's model [3], solution film heat and mass transfer resistances were introduced in their model equations. The outer surface of the tube banks was assumed to be uniformly wetted and Lewis factor was assumed to be equal to unity. However, the conditions of non-unity values of Lewis factor and incomplete surface wetting conditions were observed and addressed by many investigators. Peng and Howell [6,7] had taken the effects of incomplete surface wetting conditions into their one-dimensional differential models, where the effect of non-unity values of Lewis factor and fin efficiency factor was also considered in a combined parameter. Howell et al. [8] performed simulations and experiments on a coil-type absorber using TEG as desiccant. MR was varied from 1 to 15. It was found that the experimental data could be correlated with predictions of a simulation model only if a very small fraction of the exchanger surface was supposed to be wetted by the desiccant solution. Further, some computational results of a fully three dimensional model for the coupled heat and mass transfer between a desiccant film and air in cross-flow (Park et al. [11]) showed a higher mass transfer and a lower heat transfer than observed in the experiment, indicating that a part of the fin surface was not wetted. In determining the mass transfer coefficients from experimental data, Kessling et al. [4,5] found that better results were also obtained for small MR values or with improved surface wetting conditions. By comparing the model predictions with the experimental data, Jain et al. [16] suggested two wetness factors to account for the effect of improper wetting on the heat and mass transfer performances. For simplicity, several differential models neglected the effect of the variation of solution mass flow rate on the solution mass balance equation [6–8,16] and on the energy balance equations [6–8]. Sometimes, the sensible heat of water vapor in calculating the moist air enthalpy was not accounted for [9]. Some other investigators did not distinguish the latent heat of vaporization of pure water from the enthalpy of water vapor transferred [10] or the absorption heat for water vapor into solution [16]. For better simulations, a general one-dimensional model should take into consideration the effects of the solution film heat and mass transfer resistances, non-unity values of Lewis factor, incomplete surface wetting conditions, the variation of solution mass flow rate and sensible heat of water vapor on mass and/or energy balance equations.

For optimum design of desiccant cooling systems and annual energy performance analyses, it is most desirable to obtain an analytical solution to the general differential equations. Hellmann and Grossman [3] developed an analytical model. In deduction, however, the mass transfer coefficients on the solution side and air side were assumed to be equal and the solution film heat transfer resistance was neglected. Further, the averaged heat transfer potential between the solution and the cooling or heating fluid was approximated by a logarithmic mean temperature difference. In addition, it was assumed that both the water content and enthalpy of air at the solution–air interface change linearly along the space coordinate. Khan [13] provided an easy to use model similar to the effectiveness-NTU method for a two stream counter flow heat exchanger. However, the generality of the analytical expression is not acceptable without theoretical justification. In the present study, the general differential equations were rearranged and an analytical solution was developed. For the four possible flow arrangements of the parallel/counterflow configurations and three types of commonly used liquid desiccant solutions, results of analytical solutions were compared with those of numerical integrations over a wide range of operating conditions and the agreement was found to be quite satisfactory. Further, the heat and mass transfer performances were analyzed and some guidance to improve the unit design was provided.

2. Physical model

The physical model for the internally cooled or heated liquid desiccant–air contact units can be shown schematically in Fig. 1a. In this model, a wettability factor was utilized to describe the effect of incomplete surface wetting conditions. Also, Lewis factor was not necessary set as unity even for the uniformly wetted conditions.

However, as found in many conventional practices [2–10,12–14,16,17], the following assumptions were still adopted in the present study:

(1) zero wall, air thermal and moisture diffusivity in the flow directions;

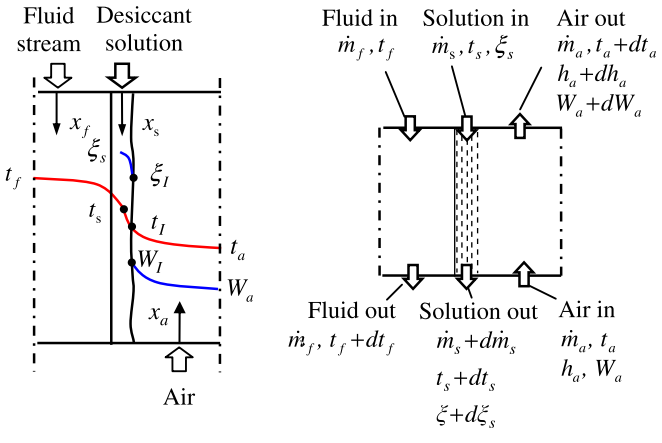

(a) Schematic of the exchanger

(b) A differential element

Fig. 1. Physical model of internally heated/cooled liquid desiccant–air contact unit.

(2) no heat transfer to the surroundings;
(3) constant specific heats of air, solution and the fluid, constant heat and mass transfer coefficients, constant surface wettability and constant Lewis factor along the height of the exchanger.

The present study was confined to the cases with mass flow rate of desiccant solution being much greater then the minimum required by the equilibrium calculation so that the changes in the concentration and the flow rate would be relatively small (e.g., with MR = 0.64–18.67 for the cases to be discussed in Section 6). For higher MR values, however, the accuracy of the analytical model to be developed would be reduced.

3. Differential equations

By principles of energy and mass conservation, a set of differential equations can be obtained for a differential element as shown in Fig. 1b as follows:

Energy balance equation for air

$$\dot{m}_a \mathrm{d}h_a = [h_G a(t_I - t_a) + h_{v,I} h_{DG} a_M (W_I - W_a)] L_a \mathrm{d}\bar{x}_a \quad (1)$$

Mass balance equation for air

$$\dot{m}_a \mathrm{d}W_a = h_{DG} a_M L_a (W_I - W_a) \mathrm{d}\bar{x}_a \quad (2)$$

Energy balance equation for fluid stream

$$\dot{m}_f c_{pf} \mathrm{d}t_f = U a_f L_f (t_s - t_f) \mathrm{d}\bar{x}_f \quad (3)$$

Energy balance equation for the differential element

$$\mathrm{d}(\dot{m}_s h_s) + \dot{m}_f c_{pf} \mathrm{d}t_f \cdot \delta_f + \dot{m}_a \mathrm{d}h_a \cdot \delta_a = 0 \quad (4)$$

Mass balance equation for the differential element

$$\mathrm{d}\dot{m}_s = -\frac{\dot{m}_s}{\xi_s} \mathrm{d}\xi_s = -\delta_a \dot{m}_a \mathrm{d}W_a \quad (5)$$

Mass balance equation for solution–air interface

$$-h_{DL} a_M (\xi_s - \xi_I) = h_{DG} a_M (W_I - W_a) \quad (6)$$

Energy balance equation for solution–air interface

$$h_L a(t_s - t_I) = h_G a(t_I - t_a) + h_{ab,I} h_{DG} a_M (W_I - W_a) \quad (7)$$

In above equations, $\mathrm{d}\bar{x}_a = \mathrm{d}x_a/L_a$, $\mathrm{d}\bar{x}_s = \mathrm{d}x_s/L_s$ and $\mathrm{d}\bar{x}_f = \mathrm{d}x_f/L_f$ represent differential dimensionless coordinates with respect to the flow lengths. For the parallel/counterflow configurations, we have $L_a = L_s = L_f = L$. $\delta_a = \mathrm{d}\bar{x}_a/\mathrm{d}\bar{x}_s$ and $\delta_f = \mathrm{d}\bar{x}_f/\mathrm{d}\bar{x}_s$ are flow direction indicators for air and fluid streams, respectively, and will be equal to ± 1, depending on the flow arrangements as shown in Fig. 2. $h_{ab,I} = h_{v,I} - \hat{h}_{w,I}$ is the heat of absorption or desorption at interface conditions.

The above equations are incomplete and other equations should be supplemented. For specific enthalpy of moist air, the following equation applies:

$$h_a = (c_{p,da} + W_a c_{pv}) t_a + W_a h_{fg,0} \quad (8)$$

For energy change of desiccant solution, the Gibbs equation applies

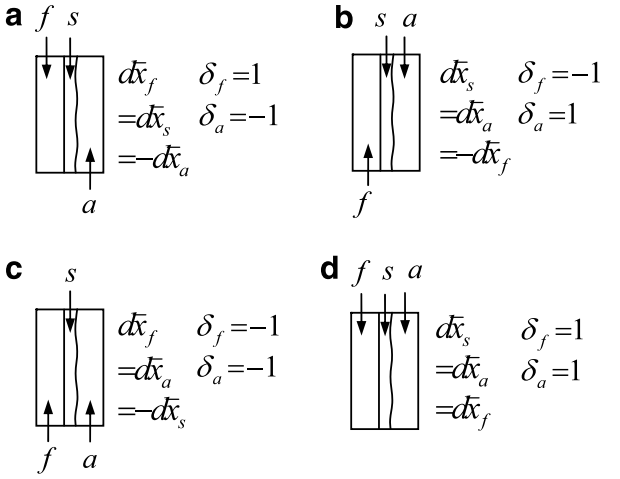

Fig. 2. Four different flow arrangements in internally heated/cooled liquid desiccant–air contact units.

$$\mathrm{d}(\dot{m}_s h_s) = \dot{m}_s c_{ps} \mathrm{d}t_s + \hat{h}_{w,s} \mathrm{d}\dot{m}_s \quad (9)$$

Eqs. (1)–(9) should be integrated subjecting to the following boundary conditions:

$$\begin{cases} t_a = t_{a,i}, W_a = W_{a,i} & \text{for } \bar{x}_a = 0 \\ t_s = t_{s,i}, \xi_s = \xi_{s,i}, \dot{m}_s = \dot{m}_{s,i} & \text{for } \bar{x}_s = 0 \\ t_f = t_{f,i} & \text{for } \bar{x}_f = 0 \end{cases} \quad (10)$$

In integration, the equilibrium humidity ratio and other properties of desiccant solution are functions of its temperature and concentration and can be calculated according to an accurately fitted equation of the published data [18,19].

4. Deduction of dimensionless differential equations

Rearrange Eqs. (1)–(4) and (8)–(9) to give

$$\mathrm{d}t_a = \frac{1}{B_1}(t_I - t_a)\mathrm{NTU}\mathrm{d}\bar{x}_a \quad (11)$$

$$\mathrm{d}W_a = (W_I - W_a)\frac{\sigma}{Le_f}\mathrm{NTU}\mathrm{d}\bar{x}_a \quad (12)$$

$$\mathrm{d}t_f = -(t_f - t_s)\frac{r}{C_f^*}\mathrm{NTU}\mathrm{d}\bar{x}_f \quad (13)$$

$$\mathrm{d}t_s = -\delta_f \frac{C_f^*}{C_s^*}\mathrm{d}t_f - \delta_a \frac{B_0}{C_s^*}\mathrm{d}t_a - \delta_a \frac{B_2 \bar{h}_{fg}}{C_s^*}\mathrm{d}W_a \quad (14)$$

In above equations, $B_0 = (1 + W_a R_{cv})$, $B_1 = B_0/[1 + R_{cv}\frac{\sigma}{Le_f}(W_I - W_a)]$ and $B_2 = (h_{v,a} - \bar{h}_{s,w})/h_{fg,0}$. $h_{v,a} = h_{fg,0} + c_{pv} t_a$ is the specific enthalpy of water vapor in air. The definitions of the other grouped parameters in Eqs. (11)–(14) are given as follows:

NTU $= (h_G a L)/(\dot{m}_a c_{p,da})$ the number of air side sensible heat transfer units;
$r = \frac{U a_f}{h_G a}$ a ratio of sensible heat transfer capacitances;
$C_s^* = \frac{\dot{m}_s c_{ps}}{\dot{m}_a c_{p,da}}$ and $C_f^* = \frac{\dot{m}_f c_{pf}}{\dot{m}_a c_{p,da}}$ solution to dry air and fluid to dry air heat capacity rate ratios, respectively;

$\bar{h}_{fg} = h_{fg,0}/c_{p,da}$ a normalized heat of evaporation at reference condition (0 °C);
$R_{cv} = c_{pv}/c_{p,da}$ water vapor to dry air specific heat capacity ratio;
$Le_f = h_G/(h_{DG}c_{p,da})$ Lewis factor for air water mixture;
$\sigma = a_M/a$ surface wettability.

The total differential of equilibrium humidity ratio is

$$dW_e = e_t dt_s + e_\xi d\xi_s \tag{15}$$

Here $e_t = \frac{\partial W_e}{\partial t_s}$ and $e_\xi = \frac{\partial W_e}{\partial \xi_s}$. For a relatively narrow range of operating conditions, the equilibrium humidity ratio can be approximated as a linear function of the solution temperature and concentration. Thus, both e_t and e_ξ can be approximated as constant coefficients for a specified application. Integrating Eq. (15) from interface to bulk solution gives an approximate relation as

$$W_s - W_I = e_t(t_s - t_I) + e_\xi(\xi_s - \xi_I) \tag{16}$$

Substitute Eq. (6) into Eq. (16) to give

$$W_s - W_I = e_t(t_s - t_I) + e_\xi R_{hD}(W_a - W_I) \tag{17}$$

Here $R_{hD} = h_{DG}/h_{DL}$ represents the ratio of gas phase mass transfer coefficient to the liquid phase mass transfer coefficient. Solving Eqs. (7) and (17) simultaneously gives

$$W_I = \frac{1}{1+P_1}W_s + \frac{P_1}{1+P_1}W_a - \frac{P_2}{1+P_1}\frac{t_s - t_a}{\bar{h}_{fg}} \tag{18}$$

$$t_I = (1-P_3)t_s + P_3 t_a - P_4\bar{h}_{fg}(W_s - W_a) \tag{19}$$

$$\mathbf{A} = (a_{ij})_{3\times 3} = \begin{pmatrix} -\left(\frac{\delta_f}{C_f^*} + \frac{1}{C_s^*}\right)r & \frac{1}{C_s^*}\left(\frac{1-P_3}{B_1}B_0 - B_2\frac{P_2}{1+P_1}\frac{\sigma}{Le_f}\right) & \frac{1}{C_s^*}\left[\frac{B_2}{1+P_1}\frac{\sigma}{Le_f} - \frac{B_0P_4}{B_1}\right] \\ \frac{r}{C_s^*} & -\left(\frac{B_0}{C_s^*} + \delta_a\right)\frac{1-P_3}{B_1} + \frac{B_2P_2}{C_s^*(1+P_1)}\frac{\sigma}{Le_f} & \left(\frac{B_0}{C_s^*} + \delta_a\right)\frac{P_4}{B_1} - \frac{B_2}{C_s^*(1+P_1)}\frac{\sigma}{Le_f} \\ \frac{e_t\bar{h}_{fg}}{C_s^*}r & -\frac{e_t\bar{h}_{fg}}{C_s^*}\frac{B_0(1-P_3)}{B_1} + B_3\frac{P_2}{1+P_1}\frac{\sigma}{Le_f} & \frac{e_t\bar{h}_{fg}B_0P_4}{C_s^*B_1} - \frac{B_3}{1+P_1}\frac{\sigma}{Le_f} \end{pmatrix} \tag{27}$$

Here

$$P_1 = -e_\xi R_{hD} + \frac{h_{ab,I}}{h_{fg,0}}\frac{\sigma}{Le_f}P_2$$

$$P_2 = e_t\bar{h}_{fg}\frac{R_h}{1+R_h}$$

$$P_3 = \frac{1 - e_\xi R_{hD}}{(1+P_1)e_t\bar{h}_{fg}}P_2$$

$$P_4 = \frac{P_1 + e_\xi R_{hD}}{(1+P_1)e_t\bar{h}_{fg}}$$

$$R_h = h_G/h_L$$

Substitute Eqs. (18) and (19) into Eqs. (11) and (12) to give

$$dt_a = \frac{1}{B_1}\left[(1-P_3)(t_s - t_a) - P_4\bar{h}_{fg}(W_s - W_a)\right]NTUd\bar{x}_a \tag{20}$$

$$dW_a = \left[-\frac{P_2}{(1+P_1)\bar{h}_{fg}}(t_s - t_a) + \frac{1}{1+P_1}(W_s - W_a)\right]\frac{\sigma}{Le_f}NTUd\bar{x}_a \tag{21}$$

Substituting Eq. (5) into Eq. (15) gives

$$dW_s = e_t dt_s + \delta_a\xi_s m_R e_\xi dW_a \tag{22}$$

Here $m_R = \frac{\dot{m}_a}{\dot{m}_s}$ represents the air to solution mass flow rate ratio.

Let's define dimensionless temperature as

$$\vartheta = t/\bar{h}_{fg} \tag{23}$$

Further define three new grouped parameters as

$$\Delta\vartheta_{fs} = \vartheta_f - \vartheta_s, \quad \Delta\vartheta_{sa} = \vartheta_s - \vartheta_a \quad \text{and} \quad \Delta W_{sa} = W_s - W_a \tag{24}$$

Using these definitions to rearrange Eqs. (13)–(14) and (20)–(22), we can get the following set of differential equations:

$$\frac{d}{dNTU_x}\mathbf{Y} = \mathbf{A}\mathbf{Y} \tag{25}$$

In this matrix equation, $dNTU_x = NTUd\bar{x}_s$, the variable vector $\mathbf{Y}$ represents a set of newly defined parameters in Eq. (24)

$$\mathbf{Y} = (\Delta\vartheta_{fs}, \Delta\vartheta_{sa}, \Delta W_{sa})^T \tag{26}$$

and $\mathbf{A}$ represents the coefficients matrix

Here $B_3 = \delta_a + \frac{e_t\bar{h}_{fg}}{C_s^*}B_2 - \xi_s m_R e_\xi$.

The boundary conditions of Eq. (10) are rewritten in dimensionless form as

$$\begin{cases} \vartheta_a = \vartheta_{a,i}, \quad W_a = W_{a,i} \quad \text{for} \quad \bar{x}_a = 0 \\ \vartheta_s = \vartheta_{s,i}, \quad \xi_s = \xi_{s,i}, \quad m_R = m_{R,i} \quad \text{for} \quad \bar{x}_s = 0 \\ \vartheta_f = \vartheta_{f,i} \quad \text{for} \quad \bar{x}_f = 0 \end{cases} \tag{28}$$

5. Analytical approach

Generally, all the elements in the coefficients matrix can be approximated as constants. From assumptions in Section 2, we can see that parameters r, C_f^*, σ, Le_f, R_h, R_{hD} and $\bar{h}_{fg}$ are constants. The changes of the mass flow rate and the concentration of the desiccant solution are usually small and the values of these variables appeared in above equations can be evaluated as the averaged values. B_0, B_1

and B_2 are approximately equal to unity and can also be approximated as constants too. By above approximations, Eq. (25) represents a set of linear and homogeneous ordinary differential equations and can be solved analytically subjecting to the boundary condition of Eq. (28).

For Eq. (25), the characteristic equation is as following:

$$|\lambda\mathbf{E}-\mathbf{A}|=0 \tag{29}$$

Within the practical range of the operating conditions, numerical calculation shows that the solution of this characteristic equation will give three different real roots. Thus, the analytical solution of Eq. (25) can be expressed as follows:

$$\mathbf{Y}=\mathbf{K}(C_1e^{\lambda_1 NTU_x},C_2e^{\lambda_2 NTU_x},C_3e^{\lambda_3 NTU_x})^T \tag{30}$$

The elements of coefficients matrix $\mathbf{K}=(k_{ij})_{3\times3}$ can be determined by the following equation:

$$(\lambda_i\mathbf{E}-\mathbf{A})(k_{1i},k_{2i},k_{3i})^T=\mathbf{0} \tag{31}$$

By satisfying Eq. (30) to the top boundary condition, i.e., for $NTU_x=0$, $\mathbf{Y}=\mathbf{Y}_T$, we can get

$$(C_1,C_2,C_3)^T=\mathbf{K}^{-1}\mathbf{Y}_T \tag{32}$$

Here $\mathbf{Y}_T=(\Delta\vartheta_{fs,T},\Delta\vartheta_{sa,T},\Delta W_{sa,T})^T$. By substituting Eq. (32) into Eq. (30), we get

$$\mathbf{Y}=\mathbf{Ke}(NTU_x)\mathbf{K}^{-1}\mathbf{Y}_T \tag{33}$$

where

$$\mathbf{e}(NTU_x)=\begin{pmatrix} e^{\lambda_1 NTU_x} & & \mathbf{0} \\ & e^{\lambda_2 NTU_x} & \\ \mathbf{0} & & e^{\lambda_3 NTU_x}\end{pmatrix} \tag{34}$$

Setting $NTU_x=NTU$ in Eq. (33), we can get the function vector at the heat exchanger's bottom position as

$$\mathbf{Y}_B=\mathbf{BY}_T \tag{35}$$

where the coefficients matrix $\mathbf{B}$ is defined as

$$\mathbf{B}=(b_{ij})_{3\times3}=\mathbf{Ke}(NTU)\mathbf{K}^{-1} \tag{36}$$

With known inlet conditions Eqs. (28) and (35) correlates five unknown variables $\vartheta_{f,o}$, $\vartheta_{s,o}$, $W_{s,o}$, $\vartheta_{a,o}$ and $W_{a,o}$ in three linear algebraic equations. In order to solve for these variables, other confinements should be imposed. Integrating Eq. (22) and rewriting the resultant equation in dimensionless form give an expression for the equilibrium humidity ratio as follows:

$$W_{s,x}=d+e_t\bar{h}_{fg}\vartheta_{s,x}+D_0(W_{a,x}-W_{a,T}) \tag{37}$$

Here, d is a constant and $D_0=\delta_a\cdot(\xi_s m_R e_\xi)_{av}$. Integrating Eq. (14) and rewriting the resultant equation in dimensionless form give an energy balance equation as follows:

$$C_s^*(\vartheta_{s,x}-\vartheta_{s,i})+C_f^*\delta_f(\vartheta_{f,x}-\vartheta_{f,T})+B_0\delta_a(\vartheta_{a,x}-\vartheta_{a,T})+B_2\delta_a(W_{a,x}-W_{a,T})=0 \tag{38}$$

Substituting Eq. (37) for bottom position into Eq. (35) can eliminate $W_{s,o}$ in the equations. By combining the resultant equations with Eq. (38) for bottom position, the following set of equations can be obtained after some rearrangements:

$$\mathbf{F}(\vartheta_{f,o},\vartheta_{s,o},\vartheta_{a,o},W_{a,o})^T=\mathbf{g} \tag{39}$$

where the expressions for coefficients matrix $\mathbf{F}$ and vector $\mathbf{g}$ for different flow arrangements are given in Appendix A. Solving Eq. (39) will give the dimensionless outlet parameters to be determined. If parameter distribution needs to be calculated, Eq. (33) should only be solved explicitly using dimensionless parameters vector $\mathbf{Y}_T$ as input parameters, which can be determined from given values or analytical results of parameters at the top position of the exchanger. This solution gives the dimensionless parameters defined in Eq. (24) at any local positions. Further, Eq. (37) can be rewritten as

$$W_{a,x}=W_{a,T}+(\Delta W_{sa}-d-e_t\bar{h}_{fg}\vartheta_{s,x}+W_{a,T})/(D_0-1) \tag{40}$$

Substituting Eq. (40) into Eq. (38) and rearranging the resultant equation will give an equation for calculating $\vartheta_{s,x}$ as follows:

$$\vartheta_{s,x}=\left(G_1-C_f^*\delta_f\Delta\vartheta_{fs}+B_0\delta_a\Delta\vartheta_{sa}-\frac{B_2\delta_a}{D_0-1}\Delta W_{sa}\right)\Big/G_2 \tag{41}$$

where $G_1=C_s^*\vartheta_{s,T}+C_f^*\delta_f\vartheta_{f,T}+B_0\delta_a\vartheta_{a,T}-\frac{B_2\delta_a}{D_0-1}(W_{a,T}-d)$

$$G_2=C_s^*+C_f^*\delta_f+B_0\delta_a-e_t\bar{h}_{fg}\frac{B_2\delta_a}{D_0-1}$$

Based on the analytical results of parameters defined in Eq. (24) and $\vartheta_{s,x}$, other dimensionless parameters such as $\vartheta_{f,x}$, $\vartheta_{a,x}$ and $W_{a,x}$ can be easily calculated.

6. Solution procedures

For a given set of control parameters ($\dot{m}_{R,i}$ or $C_{s,i}^*$, C_f^*, r, σ/Le_f, R_h, R_{hD} and NTU) and inlet conditions, it will still be necessary to evaluate at first the constants and coefficients d, e_t, e_ξ, D_0, $m_{R,av}$ or $C_{s,av}^*$, B_0–B_3, P_1–P_4 for an analytical solution. In evaluating the values of $m_{R,av}$ or $C_{s,av}^*$, B_0–B_3, P_1 and P_4, the arithmetic mean values of temperatures, concentrations and humidity ratios at extremity conditions are used. d, e_t, e_ξ and D_0 are evaluated according to the following equations:

$$e_t=[W_s(t_{s,max},\xi_{max})+W_s(t_{s,max},\xi_{min})-W_s(t_{s,min},\xi_{max})-W_s(t_{s,min},\xi_{min})]/[2(t_{s,max}-t_{s,min})] \tag{42}$$

$$e_\xi=[W_s(t_{s,max},\xi_{max})+W_s(t_{s,min},\xi_{max})-W_s(t_{s,max},\xi_{min})-W_s(t_{s,min},\xi_{min})]/[2(\xi_{max}-\xi_{min})] \tag{43}$$

$$d=[W_s(\xi_{s,i},t_{s,max})+W_s(\xi_{s,i},t_{s,min})+W_s(\xi_{s,i},t_{s,av})]/3-e_t t_{s,av} \tag{44}$$

$$D_0=\delta_a e_\xi\xi_{s,i}\frac{m_{R,i}}{1-m_{R,i}(W_{a,o}-W_{a,i})} \tag{45}$$

Here, $t_{s,av}=(t_{s,max}+t_{s,min})/2$.

Table 1
The procedure for the iterative processes of an analytical solution

Step no.	Contents to be calculated/evaluated	Equations utilized
Solution procedure for outlet parameters		
1[a]	$t_{s,max}, t_{s,min}, \xi_{max}, \xi_{min}, d, e_t, e_\xi, D_0, m_{R,av}, C^*_{s,av}, B_0$–$B_3, P_1$–$P_4$	Eqs. (42)–(47) and expressions for m_R, C^*_s, B_0–B_3 and P_1–P_4
2	a_{ij} in matrix **A**	Eq. (27)
3	$\lambda_1 - \lambda_3$	Eq. (29)
4	k_{ij} in matrix **K**	Eq. (31)
5	b_{ij} in matrix **B**	Eq. (36)
6	f_{ij} in matrix **F**, g_i in vector **g**	Equations in Appendix A
7	$\vartheta_{f,o}, \vartheta_{s,o}, \vartheta_{a,o}, W_{a,o}$	Eq. (39)
8	$t_{f,o}, t_{s,o}, t_{a,o}, \xi_{s,o}$	Eq. (23) and expression for $\xi_{s,o}$
9	Repeat steps 1–8 until converged results of outlet parameters are obtained	
Solution procedure for parameter profiles		
10	$\Delta\vartheta_{fs}, \Delta\vartheta_{sa}, \Delta W_{sa}$	Eq. (33)
11	$\vartheta_{s,x}$	Eq. (41)
12	$W_{a,x}$	Eq. (40)
13	$\vartheta_{f,x}, \vartheta_{a,x}$	Eq. (24)
14	$t_{f,x}, t_{a,x}, \quad t_{s,x}$	Eq. (23)

[a] Initially, let $t_{a,o} = t_{a,i}$, $W_{a,o} = W_{a,i}$, $t_{s,min} = t_{s,o} = t_{s,i}$, $\xi_{min} = \xi_{s,o} = \xi_{s,i}$, $t_{s,max} = t_{s,min}+1$ and $\xi_{max} = \xi_{min}+ 0.001$ for an arbitrary evaluation.

In calculation, ξ_{min}, ξ_{max}, $t_{s,min}$ and $t_{s,max}$ are to be evaluated either. Though generally the solution is either cooled or heated, the extremity values of desiccant solution temperatures will not always be found at the inlet and outlet positions. A vertex point of $t_{s,x}$ (also $\vartheta_{s,x}$) may happen at a position with the corresponding NTU_x being located in the open interval $(0, NTU)$. Thus, a special scheme is needed for finding the possible vertex point. For this purpose, Eq. (41) is differentiated with respect to NTU_x to give:

$$\frac{d\vartheta_{s,x}}{dNTU_x} = -\frac{1}{G_2}\left(C^*_f\delta_f\frac{d\Delta\vartheta_{fs}}{dNTU_x} - B_0\delta_a\frac{d\Delta\vartheta_{sa}}{dNTU_x} + \frac{B_2\delta_a}{D_0-1}\frac{d\Delta W_{sa}}{dNTU_x}\right) \quad (46)$$

The differential terms on the right hand side of Eq. (46) can be calculated according to an equation obtained by differentiating Eq. (33) as follows:

$$\frac{d\mathbf{Y}}{dNTU_x} = \mathbf{K}\frac{d\mathbf{e}(NTU_x)}{dNTU_x}\mathbf{K}^{-1}\mathbf{Y}_T \quad (47)$$

For the possible vertex point of $\vartheta_{s,x}$, $\frac{d\vartheta_{s,x}}{dNTU_x}$ should be equal to zero and this position can be found using the binary search algorithm. Values of $t_{s,min}$ and $t_{s,max}$ are determined by comparing the values of bulk solution and interface temperatures at the endpoints and the possible vertex point inside the closed interval $[0, NTU]$ (if it exists). For practical dehumidification and regeneration processes, the solution is either diluted or concentrated. Thus, the ξ_{min} and ξ_{max} are determined by comparing the values of bulk solution and interface concentrations at the same positions. In calculation, the outlet concentration can be calculated as $\xi_{s,o} = \xi_{s,i}/[1 - m_{R,i}(W_{a,o} - W_{a,i})]$ and interface parameters can be calculated using Eqs. (6), (18) and (19).

In above evaluations, outlet parameters are needed. Thus, an iterative procedure will be utilized for an analytical solution. Usually, 3–5 steps in iteration will be needed. Based on above discussions, a procedure for the iterative processes of the analytical solution is presented in Table 1.

7. Comparison and analysis

In order to demonstrate the validity of the analytical approach, results of analytical solutions and numerical integrations were compared for a set of typical operating conditions using three different desiccant solutions (LiBr, LiCl, $CaCl_2$). Much accurate solutions of differential equations (1)–(10) can be obtained through numerical integration. In calculation, Eqs. (11)–(14) are used instead of Eqs. (1)–(4) and (9) for convenience. For analytical solution, constant approximations of $m_{R,av}$ or $C^*_{s,av}$, B_0, B_1, B_2, P_1, P_2, P_3 and P_4 and linear approximation of saturation humidity were adopted. These were the only differences between the analytical solutions and numerical integrations. For comparison, a base case condition was selected as with $t_{f,i} = 20$ °C, $t_{s,i} = 30$ °C, $\xi_i = 35\%$, $t_{a,i} = 35$ °C, $W_{a,i} = 0.02155$ kg/kg (a), $C^*_f = 4$, $C^*_{s,i} = 0.5$, $r = 8$, $R_h = 0$, $R_{hD} = 0$, $\sigma/Le_f = 1$ and $NTU = 3$, using the aqueous LiCl solution. Other cases were obtained by varying a variable or two from low to high values at a time. The ranges of these variables were selected as to include most of the cases usually encountered in practical applications or for theoretical investigation purposes as follows: $t_{f,i} = 20$–65 °C, $C^*_f = 2$–16, $t_{s,i} = 25$–55 °C, $\xi_i = 10$–55%, $C^*_{s,i} = 0.15$–4, $t_{a,i} = 25$–45 °C, $W_{a,i} = 0.01095$–0.03289, $r = 2$–64, $R_h = 0$–1 and $R_{hD} = 0$–5000, $\sigma/Le_f = 0.5$–1.5 and $NTU = 0.2$–10.0. Relative errors for outlet concentration of solution, outlet humidity and enthalpy of air were defined as the ratios of the difference between the analytical and the numerical results to the overall changes by numerical integrations (see in Table 2 for the mathematical expressions). Firstly, comparison was made for the four different flow arrangements of Fig. 2 under the base case

Table 2
Comparison of outlet parameters from analytical model and numerical integration for flow arrangement of Fig. 2a

Given conditions														Analytical results					Numerical integration					Effectiveness		Rel. errors		
Case no.	Salt	$t_{f,i}$ (°C)	$t_{s,i}$ (°C)	$\xi_{s,i}$ (%)	$t_{a,i}$ (°C)	$W_{a,i}$ kg/kg(a)	$C^*_{f,i}$	$C^*_{s,i}$	r	R_h	R_{hD}	$\frac{\sigma}{Le_f}$	NTU	$t_{f,o}$ (°C)	$t_{s,o}$ (°C)	$\xi_{ss,o}$ (%)	$t_{a,o}$ (°C)	$W_{a,o}$ kg/kg(a)	$t_{f,o}$ (°C)	$t_{s,o}$ (°C)	$\xi_{ss,o}$ (%)	$t_{a,o}$ (°C)	$W_{a,o}$ kg/kg(a)	ε_W	ε_h	e_ξ (%)	e_W (%)	e_h (%)
1	LiCl	20	30	35	35	0.02155	4	0.5	8	0	0	1	3	31.46	34.22	32.32	25.53	0.00675	31.47	34.12	32.33	25.4	0.00679	0.848	0.796	−0.37	−0.27	−0.07
2	LiCl	20	30	35	35	0.02155	4	0.5	8	0	0	1	0.2	22.41	27.43	34.48	33.69	0.01887	22.41	27.47	34.48	33.7	0.01887	0.154	0.137	0.00	0.00	0.13
3	LiCl	20	30	35	35	0.02155	4	0.5	8	0	0	1	10	33.87	35.99	31.89	21.74	0.00411	33.63	35.67	31.97	21.53	0.0046	0.974	0.955	−2.64	−2.89	1.81
4	LiCl	20	30	35	35	0.02155	4	0.5	8	0	0	0.5	3	29.88	31.85	32.84	25.35	0.00977	29.91	31.83	32.83	25.31	0.00977	0.677	0.671	0.46	0.00	−0.10
5	LiCl	20	30	35	35	0.02155	4	0.5	8	0	0	1.5	3	32.06	35.51	32.13	25.39	0.00559	32.05	35.35	32.15	25.15	0.00573	0.909	0.845	−0.70	−0.88	0.22
6	LiCl	20	30	35	35	0.02155	4	0.5	8	0	5000	1	3	28.11	29.58	33.43	24.88	0.01319	28.15	29.56	33.42	24.91	0.01312	0.484	0.535	0.63	0.83	−0.46
7	LiCl	20	30	35	35	0.02155	4	0.5	8	0.3	0	1	3	29.89	31.83	32.60	28.7	0.00843	30.02	31.87	32.57	28.74	0.00823	0.765	0.678	1.23	1.50	−1.16
8	LiCl	20	30	35	35	0.02155	4	0.5	8	0.3	5000	1	3	27.12	28.29	33.61	26.92	0.01415	27.14	28.27	33.60	26.98	0.01412	0.427	0.457	0.71	0.40	−0.05
9	LiCl	20	30	35	35	0.02155	4	0.5	2	0	0	1	3	29.32	36.90	32.56	28.87	0.00817	29.34	36.74	32.57	28.77	0.00822	0.766	0.678	−0.41	−0.38	0.06
10	LiCl	20	30	35	35	0.02155	4	0.5	32	0	0	1	3	32.18	32.97	32.25	24.45	0.00633	32.18	32.93	32.26	24.31	0.00638	0.871	0.832	−0.36	−0.33	−0.03
11	LiCl	20	30	35	35	0.02155	4	0.15	8	0	0	1	3	31.23	33.38	27.73	25.69	0.00749	31.23	33.17	27.77	25.42	0.00759	0.802	0.761	−0.55	−0.72	−0.05
12	LiCl	20	30	35	35	0.02155	4	4.0	8	0	0	1	3	29.65	31.59	34.65	27.41	0.00728	29.66	31.61	34.65	27.38	0.00728	0.820	0.741	0.00	0.00	−0.07
13	LiCl	20	30	35	35	0.02155	16	0.5	8	0	0	1	3	23.37	28.05	32.17	23.25	0.00582	23.36	28.04	32.18	23.17	0.0059	0.899	0.872	−0.35	−0.51	0.23
14	LiCl	20	30	35	35	0.02155	2	0.5	8	0	0	1	3	37.91	39.05	32.59	28.69	0.00837	38.01	38.99	32.59	28.59	0.00834	0.759	0.676	0.00	0.23	−0.45
15	LiCl	20	30	35	35	0.03289	4	0.5	8	0	0	1	3	36.36	39.92	30.77	27.6	0.00835	36.36	39.66	30.79	27.28	0.00847	0.849	0.793	−0.48	−0.49	−0.04
16	LiCl	20	30	35	35	0.01059	4	0.5	8	0	0	1	3	26.46	28.06	34.02	23.75	0.00543	26.48	28.09	34.02	23.7	0.00544	0.798	0.778	0.00	−0.19	−0.10
17	LiCl	20	30	35	25	0.01913	4	0.5	8	0	0	1	3	28.58	30.66	32.64	23.98	0.00619	28.56	30.57	32.64	23.89	0.0062	0.863	0.788	0.00	−0.08	−0.20
18	LiCl	20	30	35	45	0.02155	4	0.5	8	0	0	1	3	33.24	36.4	32.37	26.72	0.00704	33.29	36.32	32.38	26.56	0.00709	0.831	0.799	−0.38	−0.35	−0.07
19	LiCl	20	30	40	35	0.02155	4	0.5	8	0	0	1	3	32.71	36.08	36.7	25.75	0.00478	32.71	35.94	36.71	25.57	0.00487	0.882	0.822	−0.30	−0.54	0.09
20	LiCl	20	30	10	35	0.02155	4	0.5	8	0	0	1	3	26.26	27.30	9.65	24.07	0.01647	26.32	27.4	9.64	24.03	0.01638	0.603	0.657	2.78	1.74	−1.10
21	LiCl	20	25	35	35	0.02155	4	0.5	8	0	0	1	3	31.14	33.97	32.3	24.92	0.00650	31.17	33.89	32.31	24.79	0.00657	0.860	0.816	−0.37	−0.47	0.09
22	LiCl	20	35	35	35	0.02155	4	0.5	8	0	0	1	3	31.76	34.43	32.35	26.15	0.007	31.77	34.35	32.35	25.99	0.00703	0.834	0.776	0.00	−0.21	−0.19
23	LiCl	65	45	35	35	0.02155	4	0.5	8	0	0	1	3	51.37	49.88	37.56	55.21	0.03352	51.61	50.1	37.46	55.16	0.03307	0.329	0.415	−4.07	−3.91	2.38
24	LiCl	65	55	35	35	0.02155	4	0.5	8	0	0	1	3	52.01	50.68	37.69	55.85	0.03399	51.97	50.44	37.71	55.92	0.03406	0.357	0.442	0.74	0.56	−0.47
25	LiCl	65	55	35	35	0.02155	64	2	64	0	0	1	3	63.17	61.92	36.53	62.21	0.05069	63.15	61.92	36.56	62.18	0.05125	0.848	0.862	1.92	1.89	−1.34
26	LiBr	65	55	50	35	0.02155	4	0.5	8	0	0	1	3	53.67	52.30	52.26	56.98	0.03154	53.66	52.13	52.26	57.04	0.03156	0.365	0.476	0.00	0.20	−0.23
27	LiBr	20	30	50	35	0.02155	4	0.5	8	0	0	1	3	31.31	34.14	46.88	25.41	0.00604	31.32	34.06	46.9	25.26	0.00612	0.861	0.809	−0.65	−0.52	0.10
28	$CaCl_2$	65	55	35	35	0.02155	4	0.5	8	0	0	1	3	45.60	44.30	40.60	51.35	0.04753	45.35	43.59	40.73	51.46	0.04803	0.314	0.341	2.27	1.89	−1.64
29	$CaCl_2$	20	30	35	35	0.02155	4	0.5	8	0	0	1	3	29.09	30.97	33.19	24.94	0.01092	29.13	30.95	33.18	24.88	0.01089	0.766	0.740	0.55	0.28	−0.37

Definitions for relative errors: $e_\xi = (\xi^a_o - \xi^n_o)/(\xi_i - \xi^n_o)$, $e_W = (W^n_{a,o} - W^a_{a,o})/(W^n_{a,i} - W^n_{a,o})$, $e_h = (h^n_{a,o} - h^a_{a,o})/(h^n_{a,i} - h^n_{a,o})$.
Definitions for effectiveness values: $\varepsilon_W = (W_{a,i} - W_{a,o})/(W_{a,i} - W_e(t_{f,i}, \xi_{s,i}))$, $\varepsilon_h = (h_{a,i} - h_{a,o})/(h_{a,i} - h_e(t_{f,i}, \xi_{s,i}))$.

conditions. Parameter profiles were presented in Fig. 3. From this figure, it can be apparently seen that the temperature difference between fluid stream and desiccant solution is not a simple exponential function of the space coordinate

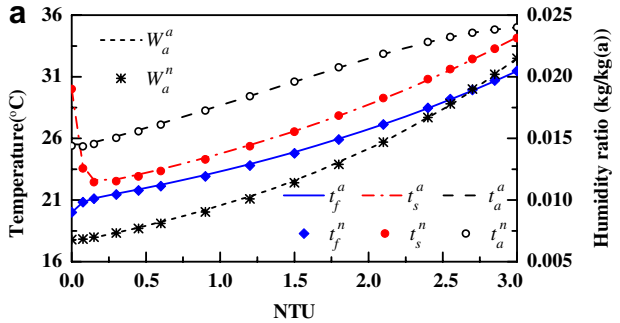

(a) For case of Fig. 2a

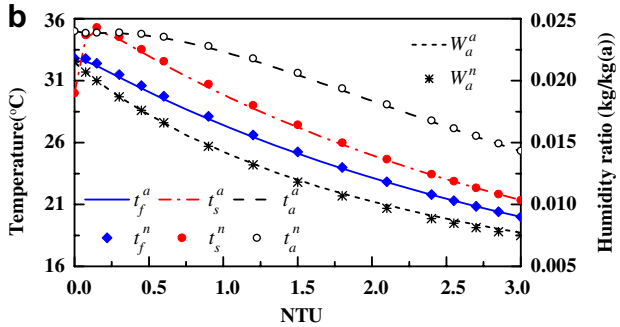

(b) For case of Fig. 2b

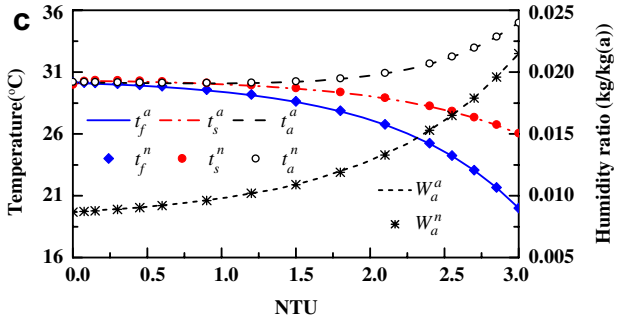

(c) For case of Fig. 2c

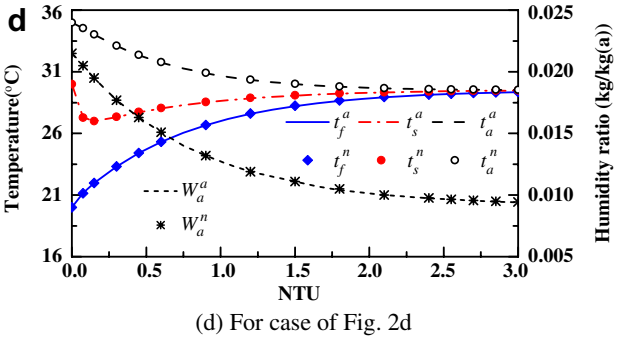

(d) For case of Fig. 2d

Fig. 3. Parameter distributions for different flow arrangements using LiCl solutions under a typical condition with $t_{f,i} = 20\ ^\circ C$, $t_{s,i} = 30\ ^\circ C$, $\xi_i = 35\%$, $t_{a,i} = 35\ ^\circ C$, $W_{a,i} = 0.02155$ kg/kg (a), $C_f^* = 4$, $C_{s,i}^* = 0.5$, $r = 8$, $R_h = 0$, $R_{hD} = 0$, $\sigma/Le_f = 1$, NTU = 3.

NTU_x. Thus, the logarithmic mean temperature difference as suggested by Hellmann and Grossman [3] is not appropriate. In addition, the interface temperature does not vary linearly with the space coordinate. Though not shown in Fig. 3, water content and enthalpy of air at the solution–air interface do not vary linearly with the space coordinate too. Nevertheless, the analytical results are in quite satisfactory agreement with the results of numerical integrations. Actually, the relative errors were found to be uniformly less than 2%. For a systematic comparison, simulation results for a set of typical operating conditions were presented in Table 2. From this table, it can be found that the maximum relative errors in absolute values are 4.07% for ξ_o, 3.91% for $W_{a,o}$ and 2.38% for $h_{a,o}$. Actually, few cases with some unconventional operating conditions have the maximum errors greater than 2%. The averaged errors are much smaller, only 0.79% for ξ_o, 0.77% for $W_{a,o}$ and 0.46% for $h_{a,o}$. This error information further shows the satisfactory agreement between the results of analytical solution and numerical integrations. Thus, the validity of the analytical method was demonstrated.

Further, the performance of the internally cooled or heated desiccant units will be analyzed briefly in the following discussions with the aid of the calculated distributions and effectiveness values. Firstly, the effect of flow arrangement on the performance of the units will be analyzed briefly. It is seen that the flow arrangement of Fig. 2a gives the highest dehumidification performance. This can be explained in terms of the averaged air side mass transfer potential, i.e., the humidity ratio difference between the air and the solution–air interface. With flow arrangement of Fig. 2a, the air flows countercurrently to the solution and fluid streams. The most humid air enters the exchanger in contact with a solution of the highest temperature and lowest concentration and, in consequence, of the highest equilibrium humidity ratio at the interface. Marching on its flowing direction, the air is kept in contact with increasingly cooler and more concentrated desiccant solution except for a small entrance region of the solution. This makes the flow arrangement of Fig. 2a have a more uniform distribution of mass transfer potential than the other flow arrangements. For similarity, the uniformity principle for the temperature difference in a heat exchanger [20] should also apply for the mass transfer potential in a mass exchanger. That is, the most uniform distribution will give the greatest averaged mass transfer potential and, in consequence, the highest dehumidification performance. For the same reason, it is easy to understand why the flow arrangement of Fig. 2d gives the lowest dehumidification performance. Similar reason can also apply for the internally heated liquid desiccant regenerators. For simplicity, later discussions on more detailed performance analysis were only made of the flow arrangement of Fig. 2a.

The unit performances can also be analyzed by their effectiveness values. In Table 2, both humidity and enthalpy effectiveness values are presented. In definitions (also shown in Table 2), the equilibrium humidity

$W_e(t_{f,i}, \xi_{s,i})$ and the equilibrium enthalpy $h_e(t_{f,i}, \xi_{s,i})$ are the extremity values that could only be reached by air through an infinitely large heat and mass exchanger. Under base case conditions (case 1) and the conditions of cases 27 and 29, the humidity effectiveness values are greater than the enthalpy ones though σ/Le_f is equal to unity. This is due to the fact that the internal heat transfer resistance from fluid to solution or solution interface causes only a relatively less significant elevation in equilibrium humidity ratio than in temperature at the interface. Thus, a less significant reduction in air side mass transfer potential than in heat transfer potential results. Increasing the internal heat transfer resistances decrease the humidity effectiveness values less significantly than the enthalpy ones (cases 7 and 9). Of course, a more significant elevation is observed in the enthalpy effectiveness value than in the humidity effectiveness value with a decreased internal heat transfer resistance (case 10). However, this phenomenon will be reversed for the regeneration applications (cases 23–26, 28). While the internal heat transfer resistances causes the internal temperature drops, the equilibrium humidity ratios at the interfaces will be more significantly reduced due to the large slopes of equilibrium humidity ratio (e_t) at high solution temperatures. Thus, special attentions should be paid to reduce the internal heat transfer resistance to improve the regenerator design (case 25). By comparing cases 1–3, it is observed that both effectiveness values decrease with the decreasing NTU values, or vice versa. With $\sigma/Le_f = 0.5$ (case 4), the air side mass transfer conductance is greatly reduced in relative to the heat transfer conductance and thus a greater reduction in the humidity effectiveness value than in the enthalpy effectiveness value results. The opposite phenomenon can be observed with $\sigma/Le_f = 1.5$ (case 5). Cases similar to those discussed in reference [3] with negligible solution film heat transfer resistances and equal mass transfer coefficients on both the solution side and air side (i.e., $R_{hD} = 1$) were also simulated. However, simulation results showed negligible effects of solution film mass transfer resistances and are thus not presented in Table 2. The reason can be given as follows. With negligible solution film heat transfer resistances, Eq. (6) can be approximately rewritten as $(W_s - W_I) = (-e_\xi R_{hD})(W_I - W_a)$. For the desiccant solutions utilized, water is easily soluble and e_ξ is much less than unity. Thus, $(W_s - W_I) \ll (W_I - W_a)$ and liquid phase mass transfer resistance can be negligible. In order to demonstrate the effect of liquid phase mass transfer resistances, a much greater mass transfer coefficient ratio of $R_{hD} = 5000$ is utilized in simulations (cases 6 and 8). Results show some more significant reductions in the humidity effectiveness value than in the enthalpy effectiveness value. Reducing the solution mass flow rate (case 11) will increase the concentration change of solution. This will reduce the averaged mass transfer potential and finally reduce the humidity effectiveness value. However, an increased humidity effectiveness value will not always be observed with an increased solution mass flow rate (case 12). Too much higher solution mass flow rate may prevent hot inlet solution to be cooled effectively. This will result in an elevated interface humidity ratio and reduce the mass transfer potential. Thus an optimum solution mass flow rate for hot inlet solution conditions exists. By comparing cases 13 and 14 with case 1, it is observed that the higher the fluid mass flow rate is, the more effectively the solution is cooled and the higher the heat and mass transfer potentials and performances result. Cases 15–22 show that both the air and solution inlet conditions affect the dehumidification performances. The hotter or the dryer the air inlet conditions, the lower the dehumidification performances due to the reduced mass transfer potential. The same reason is responsible for the lower dehumidification performances with the hotter or more dilute inlet solution conditions. Precooling or preheating the air and solution in dehumidification or regeneration units, respectively, may help to improve the unit performances. In conclusion, the humidity and enthalpy effectiveness values are affected by all the control parameters ($\dot{m}_{R,i}$ or $C^*_{s,i}$, C^*_f, r, σ/Le_f, R_h, R_{hD} and NTU) and inlet conditions. This result indicates that the easy to use model may not be appropriate for a broad range of applications as discussed above.

8. Conclusion

The characteristic of internally cooled or heated liquid desiccant–air contact units under more practical than conventional operating conditions was discussed. One-dimensional differential equations were utilized in the present study to describe the heat and mass transfer processes in such units with parallel/counterflow configurations. The effects of solution film heat and mass transfer resistances, the variation of solution mass flow rate, non-unity value of Lewis factor and incomplete surface wetting conditions were also considered in the model equations. An analytical approach was developed that combines the simplicity of solution and accuracy of a detailed model. Through comparison, results of analytical solutions were found to be in quite satisfactory agreement with those of numerical integrations.

The performances of the internally cooled or heated liquid desiccant–air contact units were also analyzed. Among the four possible flow arrangements of the parallel/counterflow configurations, the flow arrangement with air flowing countercurrently to the fluid and solution streams gives the best performance. Increasing C^*_f, r, σ/Le_f, NTU and decreasing R_h, R_{hD} increase the unit performances. However, on optimum solution mass flow rate may exist so that the air side mass transfer potential can be maximized. Special attentions should be paid to reduce the internal heat transfer resistance to improve the regenerator design. The air and solution inlet conditions also affect the unit performances too. Precooling or preheating the air and solution in dehumidification or regeneration units, respectively, will help to improve the unit performances.

Appendix A. Coefficients matrix F and vector g for Eq. (39)

For case of Fig. 2a,

$$\mathbf{F} = (f_{ij})_{4\times4} = \begin{pmatrix} 1 & -1 & b_{12} & b_{13} \\ 0 & 1 & b_{22} & b_{23} \\ 0 & e_t\bar{h}_{fg} & b_{32} & b_{33}-D_0 \\ C_f^* & C_s^* & B_0 & B_2 \end{pmatrix} \tag{A-1}$$

$$\mathbf{g} = (g_i)_4 = \begin{pmatrix} b_{11}\vartheta_{f,i} + D_1\vartheta_{s,i} + b_{13}d \\ b_{21}\vartheta_{f,i} + D_2\vartheta_{s,i} + \vartheta_{a,i} + b_{23}d \\ b_{31}\vartheta_{f,i} + D_3\vartheta_{s,i} + (1-D_0)W_{a,i} + (b_{33}-1)d \\ C_f^*\vartheta_{f,i} + C_s^*\vartheta_{s,i} + B_0\vartheta_{a,i} + B_2W_{a,i} \end{pmatrix} \tag{A-2}$$

For case of Fig. 2b,

$$\mathbf{F} = (f_{ij})_{4\times4} = \begin{pmatrix} -b_{11} & -1 & 0 & 0 \\ -b_{21} & 1 & -1 & 0 \\ -b_{31} & e_t\bar{h}_{fg} & 0 & D_0-1 \\ C_f^* & C_s^* & B_0 & B_2 \end{pmatrix} \tag{A-3}$$

$$\mathbf{g} = (g_i)_4 = \begin{pmatrix} -\vartheta_{f,i} + D_1\vartheta_{s,i} - b_{12}\vartheta_{a,i} - b_{13}W_{a,i} + b_{13}d \\ D_2\vartheta_{s,i} - b_{22}\vartheta_{a,i} - b_{23}W_{a,i} + b_{23}d \\ D_3\vartheta_{s,i} - b_{32}\vartheta_{a,i} + (D_0-b_{33})W_{a,i} + (b_{33}-1)d \\ C_f^*\vartheta_{f,i} + C_s^*\vartheta_{s,i} + B_0\vartheta_{a,i} + B_2W_{a,i} \end{pmatrix} \tag{A-4}$$

For case of Fig. 2c,

$$\mathbf{F} = (f_{ij})_{4\times4} = \begin{pmatrix} -b_{11} & -1 & b_{12} & b_{13} \\ -b_{21} & 1 & b_{22} & b_{23} \\ -b_{31} & e_t\bar{h}_{fg} & b_{32} & b_{33}-D_0 \\ C_f^* & C_s^* & B_0 & B_2 \end{pmatrix} \tag{A-5}$$

$$\mathbf{g} = (g_i)_4 = \begin{pmatrix} -\vartheta_{f,i} + D_1\vartheta_{s,i} + b_{13}d \\ D_2\vartheta_{s,i} + \vartheta_{a,i} + b_{23}d \\ D_3\vartheta_{s,i} + (1-D_0)W_{a,i} + (b_{33}-1)d \\ C_f^*\vartheta_{f,i} + C_s^*\vartheta_{s,i} + B_0\vartheta_{a,i} + B_2W_{a,i} \end{pmatrix} \tag{A-6}$$

For case of Fig. 2d,

$$\mathbf{F} = (f_{ij})_{4\times4} = \begin{pmatrix} 1 & -1 & 0 & 0 \\ 0 & 1 & -1 & 0 \\ 0 & e_t\bar{h}_{fg} & 0 & D_0-1 \\ C_f^* & C_s^* & B_0 & B_2 \end{pmatrix} \tag{A-7}$$

$$\mathbf{g} = (g_i)_4 = \begin{pmatrix} b_{11}\vartheta_{f,i} + D_1\vartheta_{s,i} - b_{12}\vartheta_{a,i} + b_{13}(d-W_{a,i}) \\ b_{21}\vartheta_{f,i} + D_2\vartheta_{s,i} - b_{22}\vartheta_{a,i} + b_{23}(d-W_{a,i}) \\ b_{31}\vartheta_{f,i} + D_3\vartheta_{s,i} - b_{32}\vartheta_{a,i} + (D_0-b_{33})W_{a.i} + (b_{33}-1)d \\ C_f^*\vartheta_{f,i} + C_s^*\vartheta_{s,i} + B_0\vartheta_{a,i} + B_2W_{a,i} \end{pmatrix} \tag{A-8}$$

In Eqs. (A-1)–(A-8), $D_1 = -b_{11} + b_{12} + b_{13}e_t\bar{h}_{fg}$, $D_2 = -b_{21} + b_{22} + b_{23}e_t\bar{h}_{fg}$, $D_3 = -b_{31} + b_{32} + b_{33}e_t\bar{h}_{fg}$.

References

[1] G. Scalabrin, G. Scaltriti, A liquid sorption–desorption system for air conditioning with heat at lower temperature, J. Solar Energy Eng. 112 (1990) 70–75.

[2] H.M. Hellmann, G. Grossman, Investigation of an open-cycle dehumidifier–evaporator–regenerator (DER) absorption chiller for low grade heat utilization, ASHRAE Trans. 101 (1995) 1281–1289.

[3] H.M. Hellmann, G. Grossman, Simulation and analysis of an open-cycle dehumidifier–evaporator–regenerator (DER) absorption chiller for low-grade heat utilization, Int. J. Refrig. 18 (3) (1995) 177–189.

[4] W. Kessling, E. Laevemann, C. Kapfhammer, Energy storage for desiccant cooling systems component development, Solar Energy 64 (4–6) (1998) 209–221.

[5] W. Kessling, E. Laevemann, M. Peltzer, Energy storage in open cycle liquid desiccant cooling systems, Int. J. Refrig. 21 (2) (1998) 150–156.

[6] C.S.P. Peng, J.R. Howell, Analysis and design of efficient absorbers for low-temperature desiccant air conditioners, J. Solar Energy Eng. 103 (1981) 67–74.

[7] C.S.P. Peng, J.R. Howell, The performance of various types of regenerators for liquid desiccants, J. Solar Energy Eng. 106 (1984) 133–141.

[8] J.R. Howell, E.C.H. Bantel, Design of liquid desiccant dehumidification and cooling systems, in: Solar Energy Utilization, NATO Advanced Science Institute Series, Martinus Nijhoff Publishers, 1987, pp. 374–386.

[9] A.G. Queiroz, A.F. Orlando, F.E.M. Saboya, Performance analysis of an air drier for a liquid dehumidifier solar air conditioning system, J. Solar Energy Eng. 110 (1988) 120–124.

[10] T.W. Chung, H. Wu, Comparison between spray towers with and without fin coils for air dehumidification using triethylene glycol solutions and development of the mass-transfer correlations, Ind. Eng. Chem. Res. 39 (6) (2000) 2076–2084.

[11] M.S. Park, J.R. Howell, G.C. Vliet, J. Peterson, Numerical and experimental results for coupled heat and mass transfer between a desiccant film and air in cross-flow, Int. J. Heat Mass Transfer 37 (1994) 395–402.

[12] A.Y. Khan, F.J. Sulsona, Modelling and parametric analysis of heat and mass transfer performance of refrigerant cooled liquid desiccant absorbers, Int. J. Energy Res. 22 (9) (1998) 813–832.

[13] A.Y. Khan, Cooling and dehumidification performance analysis of an internally-cooled liquid desiccant absorber, Appl. Therm. Eng. 18 (5) (1998) 265–281.

[14] W.Y. Saman, S. Alizadeh, Modelling and performance analysis of a cross-flow type plate heat exchanger for dehumidification/cooling, Solar Energy 70 (4) (2001) 361–372.

[15] W.Y. Saman, S. Alizadeh, An experimental study of a cross-flow type plate heat exchanger for dehumidification/cooling, Solar Energy 73 (1) (2002) 59–71.

[16] S. Jain, P.L. Dhar, S.C. Kaushik, Experimental studies on the dehumidifier and regenerator of a liquid desiccant cooling system, Appl. Thermal Eng. 20 (3) (2000) 253–267.

[17] A.Y. Khan, J.L. Martinez, Modelling and parametric analysis of heat and mass transfer of a hybrid liquid desiccant absorber, Energy Convers. Manage. 39 (10) (1998) 1095–1112.

[18] M.R. Patterson, H. Perez-Blanco, Numerical fits of the properties of lithium-bromide water solutions, ASHRAE Trans. 96 (2) (1988) 2059–2077.

[19] M.R. Conde, Properties of aqueous solutions of lithium and calcium chlorides: formulations for use in air conditioning equipment design, Int. J. Thermal Sci. 43 (4) (2004) 367–382.

[20] Z.Y. Guo, S.Q. Zhou, Z.X. Li, L.G. Chen, Theoretical analysis and experimental confirmation of the uniformity principle of temperature difference field in heat exchanger, Int. J. Heat Mass Transfer 45 (2002) 2119–2127.